JOURNAL OF ENERGY, MATERIALS, AND INSTRUMENTATION TECHNOLOGY

Journal Webpage https://jemit.fmipa.unila.ac.id/

Performance Evaluation of a Microcontroller-Based 350 W BLDC Motor Control System

Duwi Hariyanto[1]*, Muhammad Dianra Amani Ihsan[1], Basril Amien Mana[1], Dahril Khudni[1], Rudi Uswarman[1], Dean Corio[1], Nia Saputri Utami[1], and Indarta Kuncoro Aji[2]

1. Faculty of Industrial Technology, Institut Teknologi Sumatera; Jl. Terusan Ryacudu, Way Huwi, Kec. Jati Agung, Kabupaten Lampung Selatan, Lampung
2. Research & Technology of PT Nagara Sains Teknologi; Jl. Jend. Sudirman Lot 28, Kav 52-53, District 8, SCBD, Jakarta, Indonesia

Article Information

Article history:
Received November 21, 2025
Received in revised form April 18, 2026
Accepted April 21, 2026

Keywords: *BLDC, control system, electric vehicle, inverter, microcontroller*

Abstract

Electric vehicles are increasingly adopted as a strategic solution for reducing carbon emissions, yet their overall performance is strongly influenced by reliability, responsiveness, and energy efficiency. This study presents a performance evaluation of a microcontroller-based speed-control system for a 350 W brushless DC (BLDC) motor, developed using low-cost components with potential for local manufacturing. The proposed system incorporates a throttle input, Pulse Width Modulation (PWM) for speed regulation, three Hall-effect sensors for rotor position feedback, and an Arduino Nano controller integrated with an IR2110 driver and a three-phase HY4008 MOSFET inverter. A series of subsystem level tests, covering the power supply, control units, signal amplification, sensing, and motor operation, were conducted under no-load and loaded conditions using a 250 W generator as the mechanical load. The results indicate that the power supply remained stable within 50.5–50.7 V, and the IR2110 effectively amplified the 5.119 V PWM signal to 10.41–11.47 V. Hall sensor frequency increased from 129 Hz at 30% throttle to 179 Hz at 100% throttle, reflecting improved commutation synchronization with rising rotor speed. The motor achieved a speed increase of 90.8% from 220.7 rpm to 421.2 rpm under no-load, whereas under load it increased from 137.8 rpm to 356.4 rpm (an increase of 158.6%). These findings confirm that increasing the PWM duty cycle enhances electromagnetic torque and maintains rotor-stator synchronization across varying load conditions. The study demonstrates that a low-side PWM strategy with six-step commutation can be effectively implemented using low-cost hardware, supporting domestic innovation in electric vehicle technology and contributing to sustainable, low-emission transportation development.

Informasi Artikel

Proses artikel:
Diterima 21 November 2025
Diterima dan direvisi dari 18 April 2026
Accepted 21 April 2026

Kata kunci: *BLDC, sistem kendali, kendaraan listrik, inverter, mikrokontroler*

Abstrak

Kendaraan listrik semakin banyak diadopsi sebagai solusi strategis untuk mengurangi emisi karbon, namun kinerja keseluruhannya sangat dipengaruhi oleh keandalan, responsivitas, dan efisiensi energi. Penelitian ini menyajikan evaluasi kinerja sistem pengendalian kecepatan berbasis mikrokontroler untuk motor brushless DC (BLDC) berdaya 350 W yang dikembangkan menggunakan komponen berbiaya rendah dengan potensi untuk diproduksi secara lokal. Sistem yang diusulkan mengintegrasikan masukan throttle, Pulse Width Modulation (PWM) untuk pengaturan kecepatan, tiga sensor efek Hall sebagai umpan balik posisi rotor, serta pengendali Arduino Nano yang terhubung dengan driver IR2110 dan inverter tiga fasa berbasis MOSFET HY4008. Serangkaian pengujian pada tingkat subsistem yang mencakup catu daya, unit kendali, penguat sinyal, sistem sensor, dan operasi motor dilakukan pada kondisi tanpa beban maupun berbeban dengan menggunakan generator 250 W sebagai beban mekanis. Hasil penelitian menunjukkan bahwa catu daya tetap stabil pada rentang 50,5–50,7 V, dan IR2110 mampu memperkuat sinyal PWM sebesar 5,119 V menjadi 10,41–11,47 V. Frekuensi sensor Hall meningkat dari 129 Hz pada posisi throttle 30% menjadi 179 Hz pada throttle 100%, yang menunjukkan

* Corresponding author.
E-mail address: duwi.hariyanto@el.itera.ac.id

peningkatan sinkronisasi komutasi seiring bertambahnya kecepatan rotor. Motor mengalami peningkatan kecepatan sebesar 90,8%, dari 220,7 rpm menjadi 421,2 rpm pada kondisi tanpa beban, sedangkan pada kondisi berbeban kecepatan meningkat dari 137,8 rpm menjadi 356,4 rpm (meningkat sebesar 158,6%). Temuan ini mengonfirmasi bahwa peningkatan duty cycle PWM dapat meningkatkan torsi elektromagnetik dan mempertahankan sinkronisasi rotor–stator pada berbagai kondisi beban. Penelitian ini menunjukkan bahwa strategi PWM sisi rendah (low-side PWM) dengan komutasi enam langkah (six-step commutation) dapat diimplementasikan secara efektif menggunakan perangkat keras berbiaya rendah, sehingga mendukung inovasi dalam negeri di bidang teknologi kendaraan listrik dan berkontribusi pada pengembangan transportasi berkelanjutan yang rendah emisi.

1. Introduction

The increasing number of motor vehicles in Indonesia is predominantly driven by fuel-powered engines. This heavy reliance on fossil fuels contributes substantially to carbon dioxide (CO_2) emissions, which are a major source of air pollution, climate change, and global warming (Fitrianto, 2023). Beyond its environmental implications, dependence on fossil-based fuels imposes a significant burden on the national economy owing to fluctuations in global oil prices and potential threats to national energy security (Nur & Kurniawan, 2021). To address these challenges, the Government of Indonesia enacted Presidential Regulation No. 55 of 2019 on the Acceleration of Battery Electric Vehicle Programs for Road Transportation. This regulation promotes the development and adoption of electric vehicles (EVs) as an environmentally sustainable and energy-efficient alternative to reduce carbon emissions (Perpres, 2019). Electric vehicles and their supporting charging infrastructure offer several advantages, including higher energy conversion efficiency, zero local emissions, and low noise operation, thereby enhancing user comfort and contributing to improved environmental quality (Pauzi et al., 2020; Taamneh & Makahleh, 2025).

Brushless Direct Current (BLDC) motors are key components in electric vehicles due to their high efficiency, long service life, high starting torque, and require minimal maintenance due to the absence of brushes (Putranto et al., 2025). However, these advantages also require a speed-control system that is precise and adaptive to user input to ensure optimal motor performance under various load conditions. Therefore, a reliable, efficient, and domestically producible BLDC motor speed-control system is required (Natanael et al., 2025). Various approaches have been adopted to develop BLDC motor control systems. Sai Prasad Reddy et al. (2025) developed a control system based on Arduino Uno, ESC, and PWM signals with input from a potentiometer. This system demonstrated reliable performance in regulating the speed of the BLDC motor with visual feedback via an LCD and had advantages in terms of simplicity and energy efficiency.

In addition, the proportional integral derivative (PID) control strategy has been widely implemented to enhance speed regulation performance. Usha et al. (2021) demonstrated, based on simulation results and harmonic analysis, that PID controllers can reduce the overshoot, accelerate the rise time, and provide a more stable system response than PI controllers. Moreover, artificial intelligence-based optimization methods, such as Adaptive Tabu Search (ATS), have been applied by Pakdeeto et al. (2023) to design an optimal PID controller for BLDC motors. Their findings indicate that this approach achieves superior speed response performance compared to conventional tuning techniques. Furthermore, recent work by Rizqulloh et al. (2024) introduced a fuzzy PI-based field-oriented control (FOC) scheme for regulating the speed of a 10 kW BLDC motor. The proposed method demonstrated substantial improvements in the response time, overshoot, and steady-state error compared with traditional PI-based control approaches.

However, most of the aforementioned studies focus primarily on simulations or implementations in large-scale systems rather than on the development of compact and cost-effective solutions that can be locally manufactured for light electric vehicles (e.g., electric motorcycles or scooters). Therefore, there is a critical need to design a BLDC motor speed-control system that is not only functional and efficient but also adaptive to local requirements and capable of supporting national autonomy in automotive technology. This study investigates the performance of a 350 W BLDC motor speed-control system implemented on a microcontroller platform employing pulse-width modulation (PWM) and six-step commutation. The development process leverages the research team's prior experience in embedded control systems and mobility applications, including Raspberry Pi–based bioreactor regulation, autonomous vehicle controllers, and quadcopter control systems, which are relevant to the technological context and objectives of this research (Hariyanto et al., 2025; Istiqphara et al., 2020; Uswarman & Istiqphara, 2019). The novelty of this study lies in the integration of a PWM-based control mechanism and six-step commutation with a product-oriented design that emphasizes efficiency, affordability, and practical applicability. Accordingly, the findings of this study are expected to contribute to the advancement of BLDC motor control technology and reinforce Indonesia's progress toward achieving independence in electric vehicle–based automotive technology.

2. Methodology

The developed system constitutes a speed regulation apparatus for a Brushless Direct Current (BLDC) motor, specifically engineered for electric vehicle propulsion. As illustrated in **Figure 1**, the system operates by translating a throttle-generated analog signal into a controlled motor rotation. This user-input signal is processed by an Arduino Nano microcontroller, which subsequently generates a corresponding Pulse Width Modulation (PWM) signal. The PWM output is then amplified by an IR2110 driver module. The microcontroller precisely produces three complementary PWM signal pairs to govern the high-side and low-side switches of a three-phase inverter bridge. These signal pairs—designated for phases U (D5–D6), V (D7–D9), and W (D10–D11)—drive HY4008 MOSFETs, thereby modulating the power delivery to the three-phase windings (U, V, W) of the BLDC motor. The primary power source is a 48 V, 30 Ah lithium-ion battery. A dedicated LM2596HVS DC-DC Buck Converter is used to derive lower voltage rails from this source, supplying 12 V for the driver stage and 5 V for the microcontroller, throttle, and

integrated Hall-effect sensors. To ensure operational stability, the 350 W BLDC motor (12.5 cm radius) is equipped with three Hall-effect sensors (S1, S2, S3). These sensors provide real-time rotor position feedback, forming a critical closed-loop control mechanism for maintaining consistent rotational speed.

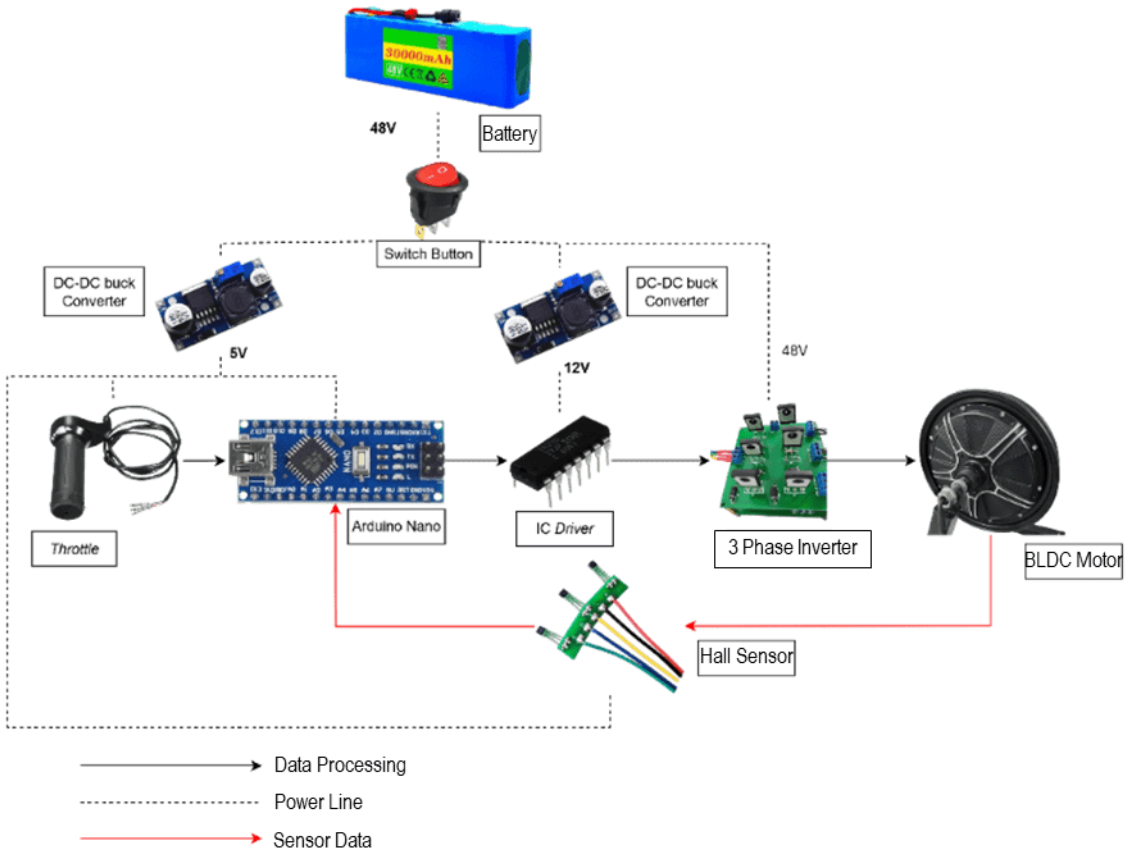

Figure 1. System block diagram

The system architecture is fundamentally organized into four principal subsystems: power supply, control, sensing, and actuation. The power supply subsystem functions to provide stable and regulated voltage and current to every component within the system. Serving as the central processing unit, the control subsystem generates Pulse Width Modulation (PWM) signals derived from throttle commands and feedback from Hall sensors. The sensing subsystem is dedicated to detecting the instantaneous rotor position, thereby establishing the precise commutation sequence. Concurrently, the actuation subsystem, implemented as a three-phase inverter, performs power conversion by transforming direct current (DC) into three-phase alternating current (AC) to energize and drive the motor. These subsystems are cohesively integrated to form a unified closed-loop speed-control system.

The flowchart of the program implemented on the microcontroller is presented in **Figure 2**. The program utilizes Hall effect sensors for rotor position detection and throttle signals for motor speed regulation via Pulse Width Modulation (PWM) duty cycle control. The algorithm reads the analog throttle value and converts it to a PWM value ranging from 0 to 255, thereby controlling the effective voltage at the low-side of the IR2110 driver. The correlation between effective voltage (V_{eff}) and input voltage (V_{in}) is defined as follows (Alsumady et al., 2021):

$$V_{eff} = \frac{dutycycle}{255} \times V_{in} \quad (1)$$

Meanwhile, three Hall effect sensors (S1, S2, S3) are employed to detect rotor position and determine the motor commutation sequence, with the specific configurations detailed in **Table 1**. Depending on the logical output combinations from these three Hall sensors, the system executes one of six distinct commutation steps (step 1 through step 6), each activating corresponding high-side and low-side transistor pairs in accordance with the three-phase motor rotation sequence (As-Salaf & Syahrial, 2021). Consequently, the motor speed is governed by the magnitude of the PWM duty cycle, whereas the rotational direction and continuity are established by the Hall sensor signal sequence. The relationship between commutation frequency (f_{comm}) and motor speed (RPM) is defined as follows:

$$f_{comm} = 6 \times pole\_pairs \times \frac{RPM}{60} \quad (2)$$

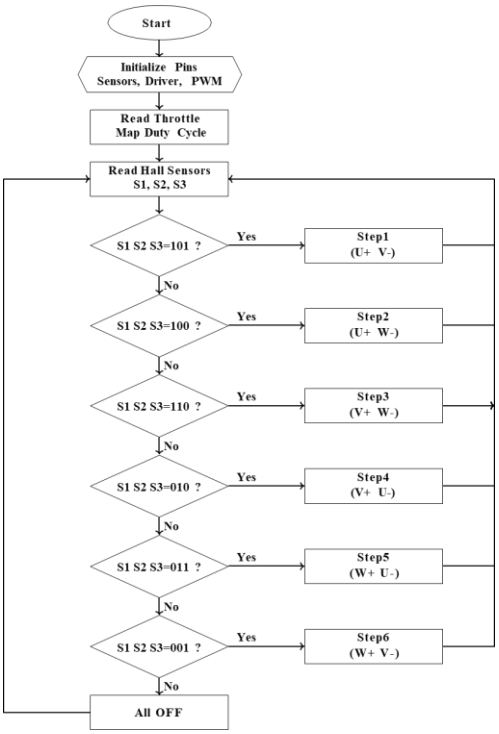

Figure 2. Flowchart of the Program

If the Hall sensor output combination deviates from all predefined patterns listed in **Table 1** (such as during rotor standstill or signal interference), all transistor outputs are disabled to prevent potential short circuits or erroneous commutation sequences.

Table 1. Motor Commutation Sequence Based on Hall Sensor Output

Hall Sensor Signal Combination			Step	Active Phase	
S1	S2	S3		High	Low
1	0	1	Step 1	U+	V−
1	0	0	Step 2	U+	W−
1	1	0	Step 3	V+	W−
0	1	0	Step 4	V+	U−
0	1	1	Step 5	W+	U−
0	0	1	Step 6	W+	V−

The testing process is carried out systematically across each subsystem. The power subsystem is examined to confirm the stability and reliability of the supply voltage. Testing of the control subsystem focuses on validating the generation of PWM signals as well as their alignment with the motor's commutation sequence. The amplifier subsystem is assessed to ensure that the MOSFET driver can adequately deliver current to the motor. Evaluation of the sensor subsystem verifies the precision of the Hall effect sensors in detecting rotor position. Finally, an integrated performance test of the entire system is performed under both no-load and loaded conditions to characterize the interplay between duty cycle, effective voltage, current, and motor rotational speed.

3. results and discussion

3.1 Power Subsystem

The experiment results showed that the 48 V lithium-ion battery was able to supply power stably to the entire control system. The output voltage of the LM2596HVS was measured at 5.0 V and 11.96 V, in accordance with the requirements of the microcontroller and the IR2110 driver. The power consumption test for each component indicated that the total system power reached 24.975 W, consisting of: the Arduino Nano at 0.15 W, three IR2110 drivers at 0.035 W, the Hall-effect sensor at 1.55 W, the throttle module at 1.95 W, and the MOSFET circuitry at 21.29 W. These results demonstrated that each component received power according to its specifications and that the power distribution system operated properly.

As shown in **Figure 3**, the battery voltage remained relatively stable within the range of 50.7 V to 50.5 V (above the nominal voltage of a lithium-ion battery, which is 48 V), while the current increased proportionally to the throttle position, as also observed in previous research (Khotimah et al., 2021). At the 10–20% throttle position, the measured current remained low at approximately 0.16 A because the motor load was not yet significant and the rotor had not fully rotated. When the throttle was increased to 30–40%, the current rose to 0.82–0.88 A, marking the initial point at which the motor began to rotate actively and the starting torque was formed. At 50–60%, the current increased to 0.94–1.01 A, and the resulting power reached around 47.5–51.1 W. When the throttle was raised to 70–80%, the system exhibited stability with a constant current of 1.01–1.02 A, indicating that the load condition had become

balanced between torque and rotational speed. At maximum throttle (90–100%), the current reached 1.10 A with a peak power of 55.55 W, while the voltage dropped only about 0.2 V from its initial value. This pattern of increasing power confirms that the supply system operated linearly with respect to throttle-position changes and was efficient in transferring electrical energy to the driver circuitry and the BLDC motor.

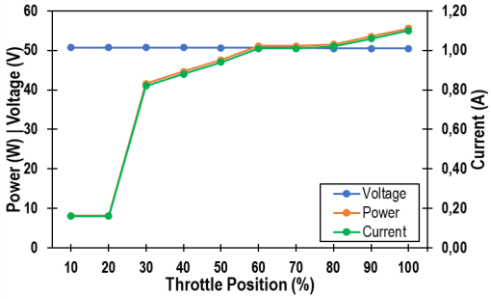

Figure 3. Test Results of Throttle Variation on Battery Voltage, Current, and Power

3.2 Microcontroller Subsystem

The testing of the Arduino Nano microcontroller showed a PWM signal with an amplitude of 5.119 V and a constant frequency of approximately 490 Hz, as presented in **Table 2**. The pulse width increased proportionally to the throttle position, demonstrating that the microcontroller was able to regulate the duty cycle effectively. With the implemented six-step configuration, each step activated one high-side (digital ON) while modulating the paired low-side, such that the three pairs of low-side PWM outputs (D6, D9, D11) determined the conduction duration of the corresponding stator coils. The low-side PWM strategy is chosen because of its implementation simplicity on a 5 V platform (Arduino Nano) and because it eliminates the need for a bootstrap circuit or complex floating high-side driver for modulation (Prawesti et al., 2021). In practice, the high-side is set to an ON state (digital HIGH) when a phase is activated, while the current duration is regulated by the PWM applied to the low-side transistor; therefore, the effective (average) coil voltage is controlled by the duty cycle according to Equation 1. This configuration also facilitates PWM signal measurement and debugging because the modulation signals reference a stable ground.

Table 2. PWM Output Signal Test Data of the Arduino Nano

Throttle (%)	PWM	Time Scale (ms)	Amplitude PWM (V)	Results
30	(Pin D5) *High side*	2	5.119	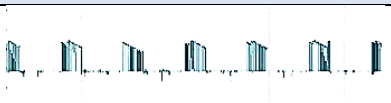
	(Pin D6) *Low side*			
	(Pin D6) *Low side (zoom in)*			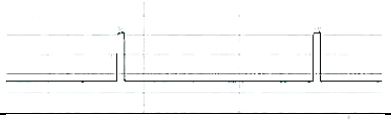
50	(Pin D5) *High side*	2	5.119	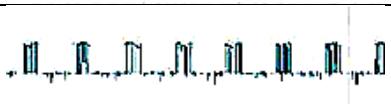
	(Pin D6) *Low side*			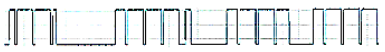
	(Pin D6) *Low side (zoom in)*			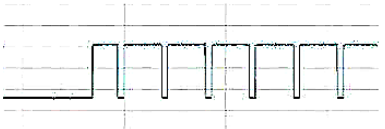
100	(Pin D5) *High side*	2	5.119	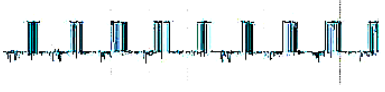
	(Pin D6) *Low side*			
	(Pin D6) *Low side (zoom in)*			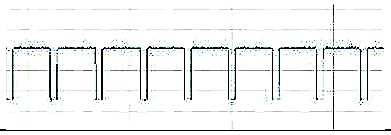

3.3 BLDC Motor Driver

The amplification circuitry in this system consists of an IR2110 driver and a three-phase inverter based on HY4008 MOSFETs. The IR2110 driver functions to amplify the PWM signal generated by the microcontroller—initially a 5 V logic signal with a low current level—into a gate-drive signal with a voltage of approximately 10–12 V and a substantially higher current capability (Fathoni et al., 2023). This amplification process is essential to ensure that the MOSFETs operate in a fully enhanced state, as the HY4008 MOSFET requires a minimum gate voltage of 10 V to achieve its lowest channel resistance (Rds(on)). Based on **Figure 4**, the IR2110 produced relatively constant high-side and low-side voltages in the range of 10.41–11.47 V. This voltage range indicates that the driver provides a voltage amplification of approximately 2.0–2.2 times the 5 V logic signal supplied by the microcontroller.

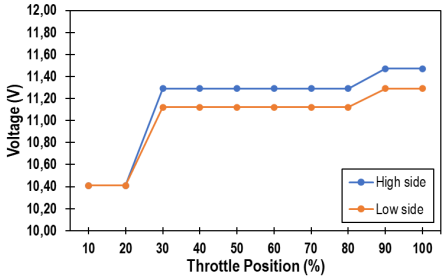

Figure 4. Measured Output Voltage of the IR2110

The variation of high-side and low-side voltages with respect to the throttle position exhibited a phenomenon consistent with the characteristics of the IR2110 driver, as shown in **Figure 4**. At the 10–20% throttle range, both the high-side and low-side voltages remained at 10.41 V because the duty cycle was very small, resulting in the bootstrap capacitor not being fully charged. When the throttle reached 30–80%, the duty cycle increased and provided a longer charging interval for the bootstrap capacitor (C_{boot}), causing the high-side gate voltage to rise to 11.12–11.29 V. At 90–100% throttle, the duty cycle reached its maximum value, placing the bootstrap charging condition at its optimum point. This caused the high-side voltage to rise to 11.47 V, slightly higher than the low-side voltage of 11.29 V, which aligns with the theory that bootstrap circuits tend to generate a slightly higher voltage than the driver supply voltage when operating at high duty cycles. Thus, these data indicate that the IR2110 operated normally, stably, and in accordance with the bootstrap-based high-side driver mode.

The output of the three-phase inverter formed by the six HY4008 MOSFETs exhibited a six-step commutation pattern with a 120° phase shift between each phase (U, V, W), as presented in **Table 3**. Evidence of this phase shift was observed in the oscilloscope waveform, where each phase was active for only 120 electrical degrees, then entered a floating state for 60°, during which the subsequent phase took over supplying current to the motor. This behavior was marked by the appearance of back electromotive force (back-EMF) in the inactive phase, which appeared as a half-sine waveform on the measurement channel (Ngadeg A. C. et al., 2022). The presence of this back-EMF serves as strong evidence that the motor operated in synchronization with the inverter commutation, and that the rotor progressed continuously following the U→V→W phase sequence.

Table 3. Output Characteristics of the HY4008 MOSFET

Throttle Position (%)	Figure	Vpp (V)	Time Scale (ms)
30%	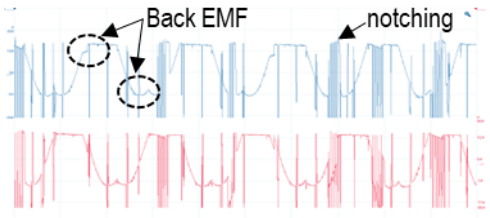	Phase U: 59.2 Phase V: 60.0	2.0
50%	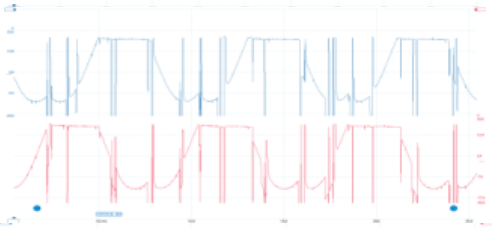	Phase U: 61.6 Phase V: 60.8	2.0
100%	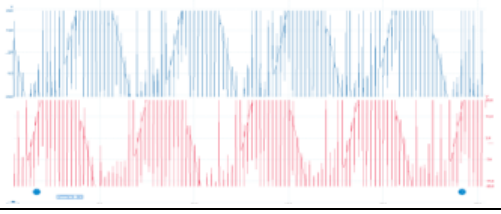	Phase U: 64.0 Phase V: 65.6	2.0

Table 3 shows the differences in waveform characteristics between low-throttle and full-throttle conditions. This indicates the direct influence of the low-side PWM modulation strategy on the effective voltage applied to the motor windings. At 30% throttle, the small duty cycle caused the low-side MOSFET to remain active only for a short duration, resulting in a modulated waveform that appeared discontinuous (notching). This occurred because the current was temporarily diverted through the freewheeling diode when the low-side was in the OFF state, while the high-side remained fully ON and therefore did not exhibit distortion. This condition produced a narrower waveform with a lower average voltage. Conversely, at 100% throttle, the duty cycle approached its maximum value, causing the low-side MOSFET to remain active for almost the entire conduction interval. This reduced the freewheeling duration and minimized notching. As a result, the waveform became fuller, smoother, and closely resembled an ideal six-step square waveform, with peak-to-peak voltages reaching 65.6 V because conduction occurred for nearly the entire commutation period.

3.4 Hall Sensor Subsystem

The test results for the Hall sensors showed that the sensors produced digital signals with a 120° phase difference, as presented in **Table 4**. Changes in throttle value had a direct effect on the frequency of the Hall sensor signals, which represent the rotor's rotational speed. Based on the test results, increasing the throttle from 30% to 50% increased the signal frequency from 129 Hz to 156 Hz, or by approximately 20.9%. A further increase to 70% resulted in a frequency of 171 Hz, indicating a 9.6% rise from the 50% condition. At the maximum throttle of 100%, the frequency reached 179 Hz, increasing by 4.7% from 70%. The accompanying reduction in period (from 7.76 ms at 30% to only 5.6 ms at 100% throttle) indicates that the rotor was spinning faster, causing the intervals between Hall signals to become shorter. This frequency change has direct implications for the six-step commutation system, because each change in the Hall sensor combination triggers a transition to the next phase in the commutation table (**Table 1**) used in the algorithm (**Figure 2**). As the frequency increases, the time available for each commutation step becomes shorter, requiring the microcontroller to respond more rapidly to maintain synchronization between the rotor position and the PWM signals supplied to the inverter. These results affirm that Hall sensors function not only as rotor position detectors, but also as indicators of actual speed that critically influence commutation rhythm and the operational stability of BLDC motors.

Table 4. Frequency and Period Data of Hall Sensors

Throttle %	Frequency (Hz)	Period (s)	Time Scale (ms)	Figure [S1 = blue, S2 = red]
30	129	7.76×10^{-3}	2×10^{-3}	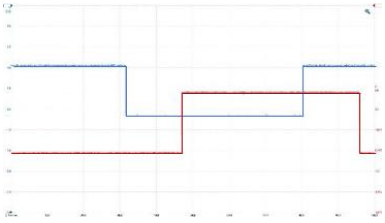
50	156	6.40×10^{-3}	2×10^{-3}	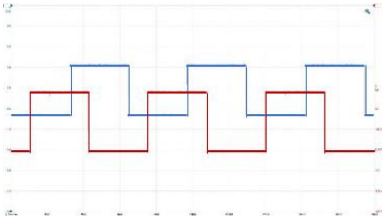
70	171	5.84×10^{-3}	2×10^{-3}	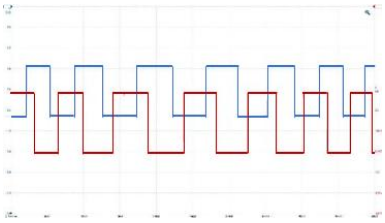
100	179	5.60×10^{-3}	2×10^{-3}	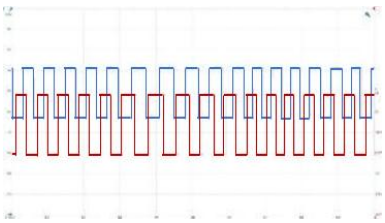

3.5 Motor Control Testing Under Load and No-Load Conditions

Motor control testing was carried out using a generator load rated at 250 W with a radius of 3 cm, connected via a belt. The results showed that throttle increments caused a significant increase in battery power, exhibiting different characteristics between the no-load and loaded conditions, as shown in **Figure 5**. Under no-load conditions, increasing the throttle from 30% to 100% raised battery power from 41.57 W to 55.55 W, or approximately 33.6%. Meanwhile, under loaded conditions, the power increased much more substantially, from 40.56 W to 105.44 W, or about 159.9%. The power surge under load occurred because the generator imposed mechanical resistance that required the motor to produce higher torque, thereby increasing the current drawn from the battery much more significantly than in the no-load condition. This phenomenon is consistent with the concept that the higher the PWM duty cycle, the greater the effective voltage applied to the motor windings, thus increasing power demand—particularly when mechanical loads convert part of the electromagnetic energy into electrical energy in the generator.

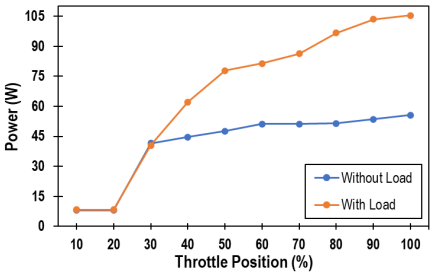

Figure 5. Battery Power Measurements Under No-Load and Load Conditions

The difference in speed response between the no-load and loaded conditions was strongly influenced by the torque demand required from the motor, as illustrated in **Figure 6**. The BLDC motor has a rotor radius of 12.5 cm, while the generator load has a radius of 3 cm. A comparison of these radii shows that the motor possesses a moment arm 4.17 times larger than that of the generator, corresponding to a 316.7% difference in mechanical leverage. This radius difference caused the generator to exert higher reactive torque on the motor at low rpm, resulting in a significant reduction in initial motor speed when the load was applied. In this case, at 30% throttle, the no-load motor speed of 220.7 rpm decreased to 137.8 rpm when the load was applied. However, as the throttle increased, the PWM duty cycle rose, the effective coil voltage increased, and the Hall sensor frequency increased, causing commutation steps to transition more rapidly. This accelerated the rotation of the stator field and forced the rotor to increase its speed to maintain synchronization with the magnetic field. As a result, although the generator load absorbed part of the energy in the form of mechanical torque, the motor speed still increased from 137.8 rpm to 356.4 rpm (a 158.6% rise) when the throttle was increased from 30% to 100%. Conversely, under no-load conditions, the torque demand was small, resulting in a speed increase of only about 90.8% across the same throttle range. These results show that the control system was able to respond to different torque requirements arising from load and radius differences, and was capable of maintaining stable commutation transitions so that the motor continued to follow the acceleration of the stator field effectively.

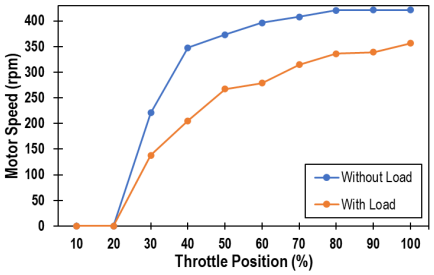

Figure 6. BLDC Motor Speed Measurements Under No-Load and Load Conditions

Overall, the performance of this microcontroller-based BLDC motor control system is determined by the linear relationship between throttle magnitude regulating PWM duty cycle, PWM determining torque and rotor acceleration, Hall sensor frequency governing commutation rhythm, and motor RPM as the final output. In this mechanism, increasing the throttle directly increases the PWM duty cycle on the low-side inverter, thereby increasing the effective voltage across the motor windings and generating greater electromagnetic torque. A similar result is also reported by Astuti & Masdi (2022). The increased torque accelerates the rotor, and this acceleration is reflected in the rising Hall sensor frequency (for example, from 129 Hz at 30% throttle to 179 Hz at 100%), indicating that rotor position changes occur more rapidly. The increase in Hall frequency requires the six-step commutation system to transition between steps in progressively shorter intervals, causing the stator magnetic field to rotate faster and the rotor to accelerate accordingly, reaching 421.2 rpm at 100% throttle. Conversely, when the throttle is decreased toward 0%, the PWM duty cycle decreases, reducing the effective voltage applied to the windings. Consequently, electromagnetic torque weakens, Hall frequency drops, the commutation rhythm slows, and the stator field rotates more slowly. The rotor then loses driving energy, RPM decreases gradually, and the motor eventually comes to a stop.

4. Conclusions

The results of this study indicate that the BLDC motor speed-control system—constructed using an Arduino Nano microcontroller, an IR2110 driver, and a three-phase MOSFET HY4008 inverter—operates stably and efficiently

in regulating motor speed in response to throttle variations. The power subsystem performs optimally, as evidenced by the stable battery voltage in the range of approximately 50.5–50.7 V and a total power consumption of approximately 25.0 W. The microcontroller generates stable PWM signals at 490 Hz with an amplitude of 5.119 V, and the IR2110 driver successfully amplifies them to 10.41–11.47 V. The three-phase inverter produces consistent six-step commutation with a 120° phase shift and peak-to-peak voltage reaching 65.6 V at 100% throttle. The Hall sensors record an increase in frequency from 129 Hz at 30% throttle to 179 Hz at 100%, confirming an accelerated commutation rhythm corresponding to rotor speed increase. Both load and no-load tests demonstrate consistent system responses to changes in mechanical torque. Under no-load conditions, battery power increases by 33.6% when the throttle is raised from 30% (41.57 W) to 100% (55.55 W). Under loaded conditions using a 250 W generator with a 3 cm radius, the power surge is significantly larger—159.9%, rising from 40.56 W to 105.44 W. This difference aligns with the higher torque demand associated with the radius difference, which has a ratio of 4.17:1. The motor speed under no-load conditions increases from 220.7 to 421.2 rpm (a 90.8% rise), whereas under load it increases from 137.8 to 356.4 rpm (a 158.6% rise). These results demonstrate that the control system is capable of increasing torque through PWM duty-cycle adjustments, which subsequently accelerate the rotor, raise the Hall sensor frequency, and accelerate the commutation rhythm, thereby maintaining motor synchrony with the stator field even under load conditions. This study demonstrates that a low-side PWM approach with six-step commutation can be effectively implemented using low-cost hardware components while still achieving stable control performance. For future development, the implementation of a closed-loop control scheme based on Proportional–Integral (PI) control or Field-Oriented Control (FOC) is recommended to improve dynamic response.

Acknowledgment

The authors express their sincere appreciation and gratitude to Lembaga Penelitian dan Pengabdian Masyarakat (LPPM) Institut Teknologi Sumatera (ITERA), for the financial support provided through the Research Program under the Scientific Group Strengthening Scheme for Fiscal Year 2025, Contract Number 2658u/IT9.2.1/PT.01.03/2025.

5. Bibliography

Alsumady, M. O., Alturk, Y. K., Dagamseh, A., & Tantawi, M. (2021). Controlling of DC-DC buck converters using microcontrollers. *International Journal of Circuits, Systems and Signal Processing, 15*, 197–202. https://doi.org/10.46300/9106.2021.15.22

As-Salaf, M. H., & Syahrial, S. (2021). Simulasi pengaturan kecepatan motor BLDC menggunakan software PSIM. *MIND Journal, 6*(1), 103–117. https://doi.org/10.26760/mindjournal.v6i1.103-117

Astuti, P., & Masdi, H. (2022). Sistem kendali kecepatan motor BLDC menggunakan PWM berbasis mikrokontroler Arduino Uno. *JTEIN: Jurnal Teknik Elektro Indonesia, 3*(1), 120–135. https://doi.org/10.24036/jtein.v3i1.216

Fathoni, K., Apriaskar, E., Salim, N. A., Sulistyawan, V. N., Satria, R. L., & Hidayat, S. (2023). Design of brushless DC motor driver based on bootstrap circuit. *Jurnal Elektronika dan Telekomunikasi, 23*(2), 108. https://doi.org/10.55981/jet.563

Fitrianto, H. (2023). Analisis penggunaan kendaraan listrik sebagai upaya penurunan emisi lingkungan: Case study kendaraan listrik di Provinsi Sumatera Utara. *Cakrawala, 6*(2), 1056–1067. https://doi.org/10.52851/cakrawala.v6i2.302

Hariyanto, D., Miranto, A., Naufal, D., Rafif, M. N., Hernanda, P., Marvie, I., & Panjaitan, J. R. H. (2025). Analisis kinerja perangkat instrumentasi dan kontrol bioreaktor Cascara berbasis Raspberry Pi. *Jurnal Teknik Elektro dan Komputasi (ELKOM), 7*(1), 54–64. https://doi.org/10.32528/elkom.v7i1.23858

Istiqphara, S., Uswarman, R., Heriansyah, & Utama. (2020). Pengendalian tracking posisi purwarupa autonomous land vehicle dengan menggunakan metode PID dan model kinematik. *Electrician, 14*(2), 34–39. https://doi.org/10.23960/elc.v14n2.2121

Khotimah, N. D., Subiyantoro, S., & Rifa'i, M. (2021). Desain sistem kontrol kecepatan motor menggunakan kendali PID pada solar e-bike. *Jurnal Elektronika dan Otomasi Industri, 8*(2), Article 11. https://doi.org/10.33795/elk.v8i2.271

Natanael, F., Arthaya, B. M., & Wahab, F. (2025). Rancang bangun sistem throttle brushless DC motor pada kursi roda elektrik. *Electron: Jurnal Ilmiah Teknik Elektro, 6*(1).

Ngadeg, A. C. M. N., Satya Kumara, I. N., & Elba Duta Nugraha, I. P. (2022). Rancang bangun controller BLDC berbasis mikrokontroler STM32 Blue Pill pada kendaraan listrik Urban Agnijaya Weimana. *Jurnal SPEKTRUM, 9*(3), 53–60. https://doi.org/10.24843/SPEKTRUM.2022.v09.i03.p7

Nur, A. I., & Kurniawan, A. D. (2021). Proyeksi masa depan kendaraan listrik di Indonesia: Analisis perspektif regulasi dan pengendalian dampak perubahan iklim yang berkelanjutan. *Jurnal Hukum Lingkungan Indonesia, 7*(2), 197–220. https://doi.org/10.38011/jhli.v7i2.260

Pakdeeto, J., Wansungnoen, S., Areerak, K., & Areerak, M. (2023). Optimal speed controller design of commercial BLDC motor by adaptive tabu search algorithm. *IEEE Access, 11*, 79710–79720. https://doi.org/10.1109/ACCESS.2023.3300233

Pauzi, G. A., Rahma, D., & Suciyati, S. W. (2020). Rancang bangun prototipe pengoptimal charging baterai pada mobil listrik dari pembangkit tenaga surya dengan menggunakan sistem boost converter. *Journal of Energy, Material, and Instrumentation Technology, 1*(2).

Peraturan Presiden Republik Indonesia Nomor 55 Tahun 2019 tentang Percepatan Program Kendaraan Bermotor Listrik Berbasis Baterai (Battery Electric Vehicle) untuk Transportasi Jalan. (2019). Pemerintah Republik Indonesia.

Prawesti, R. D., Fathoni, F., & Pracoyo, A. (2021). Rancang bangun six-step inverter 3 fasa sebagai modul pembelajaran elektronika daya. *Jurnal Elektronika dan Otomasi Industri, 8*(2), 59–66. https://doi.org/10.33795/elk.v8i2.276

Putranto, R. D., Hafidz, I., Kholima, H., & Putri, N. W. (2025). Enhancing BLDC motor performance with wheel-hub design by modifying coil configurations. *Journal of Energy, Material, and Instrumentation Technology, 6*(3). https://doi.org/10.23960/jemit.359

Rizqulloh, M. S., Pamuji, F. A., & Suryoatmojo, H. (2024). Design and simulation of 10 kW BLDC motor speed control for electric vehicles using FOC based on fuzzy logic control. *Journal on Advanced Research in Electrical Engineering, 8*(1). https://doi.org/10.12962/jaree.v8i1.386

Sai Prasad Reddy, M., Pranav, K., Rahman, W., Vijay Kumar, B., Jain, A., & A. B., G. (2025). Speed control of BLDC motor using PWM and Arduino Uno. *E3S Web of Conferences, 619*, Article 02007. https://doi.org/10.1051/e3sconf/202561902007

Taamneh, M. M., & Makahleh, H. Y. (2025). The prospects of adopting electric vehicles in urban contexts: A systematic review of literature. *Transportation Research Interdisciplinary Perspectives, 31*, 101420. https://doi.org/10.1016/j.trip.2025.101420

Usha, S., Dubey, P. M., Ramya, R., & Suganyadevi, M. V. (2021). Performance enhancement of BLDC motor using PID controller. *International Journal of Power Electronics and Drive Systems, 12*(3), 1335–1344. https://doi.org/10.11591/ijpeds.v12.i3.pp1335-1344

Uswarman, R., & Istiqphara, S. (2019). Perancangan sistem kendali quadcopter menggunakan modified sliding mode control. *Jurnal Nasional Teknik Elektro dan Teknologi Informasi, 8*(3), 273–280. https://doi.org/10.22146/jnteti.v8i3.523